A REPORT ON

GEOLOGICAL AND SEISMIC EVALUATION OF THE FEBRUARY 6, 2023 M_w 7.8 and M_w 7.7 EARTHQUAKES, AND THEIR KINEMATIC AND DYNAMIC INTERACTIONS

Contributors to the report

Prof. Dr. Erhan Altunel (Eskişehir Osmangazi University)

Prof. Dr. Ali Pinar (Kandilli Observatory and Earthquake Research Institute, Boğaziçi University)

Prof. Dr. Mustafa Erdik (Turkish Earthquake Foundation)

Prof. Dr. Sinan Akkar (T-RUPT Inc.)

GEOLOGICAL AND SEISMIC EVALUATION OF THE FEBRUARY 6, 2023 M_w 7.8 and M_w 7.7 EARTHQUAKES, AND THEIR KINEMATIC AND DYAMIC INTERACTIONS

Prof. Dr. Erhan Altunel (Eskişehir Osmangazi University)
Prof. Dr. Ali Pinar (Kandilli Observatory and Earthquake Research Institute, Boğaziçi University)
Prof. Dr. Mustafa Erdik (Turkish Earthquake Foundation)
Prof. Dr. Sinan Akkar (T-RUPT Inc.)

1.INTRODUCTION

Two large earthquakes of moment magnitudes M_w 7.8 and M_w 7.7 (based on USGS slip model solutions where the first event is revised as M_w 7.9 on 21/02/2023) occurred in southeast Turkey on February 6, 2023, at 04:17 and 13:24 (local time, +3 GMT), respectively. (Note: The second earthquake is reported as M_w 7.5 by USGS, which relies on Centroid Moment Tensor Solution. The magnitudes of first and seconds event are taken as M_w 7.8 and M_w 7.7, respectively hereafter to prevent ambiguity in the report). This report discuses and elaborates the faults ruptured by these earthquakes, their rupture mechanisms, and the historical earthquake activities on these faults. On the basis of this information, an extensive discussion and evaluation take place about the kinematic relation between the ruptured fault segments of these two major events. These discussions illuminate the level of kinematic interaction between these two faults that led the triggering of the second earthquake (M_w 7.7) by the stress transfer of the first event (M_w 7.8).

The slip model presented in this report indicate that the M_w 7.8 event that occurred on the main segments of the East Anatolian Fault Zone loaded additional stress on the Sürgü-Çardak fault. The excessive additional stress pushed forward the failure of the Sürgü-Çardak fault and its western segment ruptured creating the second major earthquake (M_w 7.7) approximately nine hours after the first one.

Table 1 and Table 2 provide the source parameters of the M_w 7.8 and M_w 7.7 earthquakes determined by different seismological agencies. The earthquake loss model of CATMOD for computing the DASK, treaty and facultative portfolio loses of Turk Reasurans Inc. used the source modeling parameters discussed in this report.

Table 1. Source parameters of the 6 February, 2023 04:17 earthquake (M_w 7.8).

Origin Time (GMT)	Lat (Deg.)	Long (Deg.)	Depth (km)	M_w	Strike1 (Deg.)	Dip1 (Deg.)	Rake1 (Deg.)	Strike2 (Deg.)	Dip2 (Deg.)	Rake2 (Deg.)	Agency
6.02.2023 01:18	37.6	37.5	15	7.8	54	70	11	320	80	160	GCMT
6.02.2023 01:18	37.4	37.8	33	7.9	234	79	14	142	76	169	USGS
6.02.2023 01:17	37.7	37.6	23	7.7	237	79	0	327	90	-169	INGV
6.02.2023 01:17	37.2	37.0	11	7.8	65	70	11	331	80	160	OCA
6.02.2023 01:17	37.8	37.6	14	7.8	56	67	11	322	80	156	CPPT
6.02.2023 01:17	37.2	37.0	10	7.7	142	86	-165	51	75	-4	GFZ
6.02.2023 01:17	37.1	37.1	10	7.7	324	65	-152	222	64	-27	KOERI
6.02.2023 01:17	37.2	37.0	13	8.0	323	72	-171	230	81	-18	IPGP
6.02.2023 01:17	37.2	37.1	18	7.8	233	74	18	140	77	168	ERD

Table 2. Source parameters of the 6 February, 2023 13:24 earthquake (M_w 7.7)

Origin Time (GMT)	Lat (Deg.)	Long (Deg.)	Depth (km)	M_w	Strike1 (Deg.)	Dip1 (Deg.)	Rake1 (Deg.)	Strike2 (Deg.)	Dip2 (Deg.)	Rake2 (Deg.)	Agency
6.02.2023 10:24	38.1	37.2	12	7.7	261	42	-8	358	84	-132	GCMT
6.02.2023 10:24	38.1	37.2	14	7.7	275	62	1	185	89	152	INGV
6.02.2023 10:24	38.5	37.9	12	7.8	256	24	-14	359	84	-114	CPPT
6.02.2023 10:24	38.1	37.2	15	7.6	359	79	178	89	88	10	GFZ
6.02.2023 10:24	38.0	37.2	10	7.7	5	70	180	275	90	20	OCA
6.02.2023 10:24	38.0	37.2	19	7.7	6	85	-172	276	82	-6	USGS
6.02.2023 10:24	38.0	37.2	13	7.7	270	60	-9	5	82	-150	IPGP
6.02.2023 10:24	38.0	37.3	10	7.6	273	67	-9	6	81	-157	KOERI
6.02.2023 10:24	38.1	37.2	16	7.6	358	73	174	90	86	13	ERD

2. SEISMOTECTONIC FRAMEWORK OF THE REGION

2.1. Introduction

The present tectonic interaction between the Arabian-African and Eurasian plates forces the Anatolian Block to move westward (Figure 1). The westward movement of the Anatolian Block mainly takes place along the North Anatolian Fault Zone (NAFZ) in the north and the East Anatolian Fault Zone (EAFZ) in the southeast. The EAFZ is a left-lateral strike slip fault and it accommodates the relative motion between the Anatolian Block and the Arabian Plate (e.g. Şengör et al., 1985; Dewey et al., 1986; Barka and Kadinsky-Cade, 1988; Barka and Reilinger, 1997). The total length of the EAFZ is about 550 km and it extends from Karlıova in the northeast to the Mediterranean Sea in the southwest. Although there is an agreement regarding the main trace of the fault zone between Karlıova in the northeast and Türkoğlu in the southwest (Figure 1), the southwestern continuation further southwest of Türkoğlu is under debate. Opinions of researchers about the

southwestern extension of the EAFZ further southwest of Türkoğlu can be compiled into three groups as summarized below.

The EAFZ intersects with the Dead Sea Fault Zone (DSFZ) around Türkoğlu and the fault zone crosses the Amanos Mountains and extends up to the Iskenderun Bay (e.g. McKenzie, 1970, 1972; Dewey et al., 1973; Şengör, 1980; Hempton, 1987; Jackson and McKenzie, 1984; Barka and Kadinsky-Cade, 1988; Kempler and Garfunkel, 1991; Westaway and Arger, 1996; Koçyiğit and Erol, 2001, Yönlü et al. 2017).

The major trace of the EAFZ extends along the Karasu Segment in the Karasu Valley to the south and it meets with the DSFZ in the Amik Basin (e.g. Allen, 1969; Arpat and Şaroğlu, 1975; Kelling et al., 1987; Şaroğlu et al., 1992; Şengör et al., 1985; Över et al., 2004; Duman and Emre, 2013).

The EAFZ terminates around Türkoğlu, it does not extend further southwest and it connects with the DSFZ through the Karasu Fault (e.g. Lovelock, 1984; Muehlberger and Gordon, 1987; Perinçek and Çemen, 1990; Chorowicz et al., 1994; Yürür and Chorowicz, 1998).

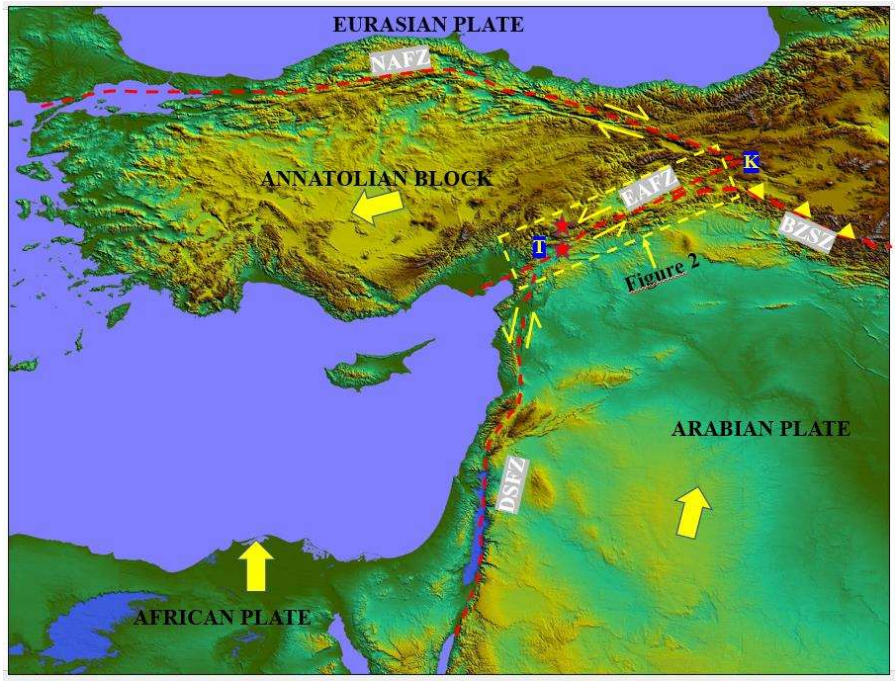

Figure 1. Simplified map of the Eastern Mediterranean showing relative plate motions (solid yellow arrows) and major active fault zones (dashed red lines). NAFZ: North Anatolian Fault Zone, EAFZ: East Anatolian Fault Zone, DSFZ: Dead Sea Fault Zone (yellow half arrows show sense of motion on the fault zone). BZSZ: Bitlis-Zagros Sture Zone (yellow triangles are on the thrusting site). K: Karlıova, T: Türkoğlu. Map produced from SRTM Worldwide Elevation Data (1-arc-second resolution).

The EAFZ is divided into fault segments in several studies (e.g. Arpat and Şaroğlu 1975; Şengör et al. 1985; Muehlberger and Gordon 1987; Şaroğlu et al. 1992). Duman and Emre (2013) segmentation model divides the EAFZ into several distinct geometric fault segments, which is in use today, based on fault step-overs, jogs or changes in fault strike (Figure 2). In this model, an EW-trending left-lateral fault splits from the EAFZ in southwest of Çelikhan and extends towards Göksun.

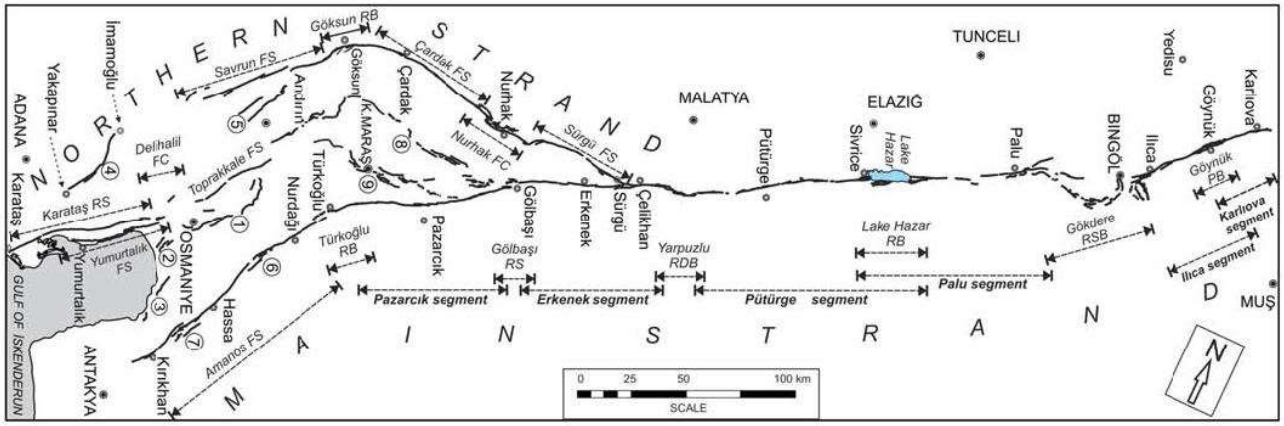

Figure 2. Map of the East Anatolian strike-slip fault system showing strands, segments and fault jogs. Abbreviations: FS, fault segment; RB, releasing bend; RS, releasing stepover; RDB, restraining double bend; RSB, restraining bend; PB, paired bend; (1) Düziçi–Osmaniye fault segment; (2) Erzin fault segment; (3) Payas fault segment; (4) Yakapınar fault segment; (5) Çokak fault segment; (6) Islahiye releasing bend; (7) Demrek restraining stepover; (8) Engizek fault zone; (9) Maraş fault zone (Duman and Emre 2013).

Different criteria including geological data (e.g. Arpat and Şaroğlu 1975, Westaway and Arger 1996, Yönlü et al. 2017), GPS data (e.g. McClusky et al. 2000, Reilinger et al. 2006), plate kinematic analysis (e.g. Lyberis et al. 1992, Yürür and Chorowicz 1998) and seismological data (Taymaz et al. 2004) suggest that the slip rate on the EAFZ ranges between 4 to 3.1 mm/yr. The amount of total offset on the EAFZ varies depending on the features of offset by the fault zone. For example, based on offset geological pinpoints, up to 27 km cumulative left-lateral offset was estimated (e.g. Arpat and Şaroğlu 1972; Şaroğlu et al. 1992). A left diversion on the Euphrates River in southwest of Elazığ was considered as a left lateral offset by Arpat and Şaroğlu (1975) and 15 km cumulative offset was estimated. Yönlü et al. (2013) suggest that the Aksu River valley is left laterally offset by the EAFZ about 16.5 ± 0.5 km.

2.2. Seismotectonics

On the main earthquake sources of the region, EAFZ and DSFZ, moderate and large earthquakes have occurred during the pre-instrumental and instrumental periods. The pre-instrumental earthquake activity of the EAFZ and DSFZ is discussed by Akyüz et al. (2006), Karabacak (2007),

Altunel et al. (2009), Yönlü (2012) and Yönlü et al. (2017), based on historical data and paleoseismological studies. Several surface rupturing events reportedly took place on the EAFZ in the 19th century (e.g. 1866 M 6.8, 1874 M ≥ 7.1, 1875 M 6.7, 1893 M 7.1 earthquakes). Ambraseys (1989) indicates that two thirds of the fault zone was ruptured during the 19th century earthquake activity (Figure 3). Earthquakes in 1114 and 1513 are most probably occurred on the southwestern part of the fault zone and caused significant damage in northern Syria and eastern Anatolia (Calvi, 1941; Soysal et al., 1981; Ambraseys, 1989). Based on paleoseismological studies, Yönlü (2012) and Yönlü et al. (2017) revealed that the 1513 (M 7.4) and 1114 earthquakes occurred on the Türkoğlu-Pazarcık and Pazarcık-Gölbaşı segments of the EAFZ, respectively. According to Ambraseys (1989), the 1544 (M = 6.7) earthquake took place on the Çardak-Sürgü Fault, which splits from the EAFZ in southwest of Çelikhan (Figure 3).

The Adana Basin has also experienced large earthquakes both in historical times and during the instrumental period (e.g. Arvanitakis, 1903; Sieberg, 1932; Calvi, 1941; Ergin et al., 2004; Soysal et al., 1981; Ambraseys, 1989; Guidoboni and Comastri, 2005). Several large or moderate-size historical earthquakes are reported in the area; for example, the 526 AD and 561 AD earthquakes caused substantial damage at the ancient cities of Anazarbus and Castabala and these major cities were abandoned after these events (Jörg, 1986). A destructive earthquake also took place in 1269 and more than 60,000 people died in the Adana Basin (Arvanitakis, 1903; Calvi, 1941; Guidoboni and Comastri, 2005). However, there is insufficient information in the literature to attribute these events to specific fault segments. Regarding the instrumental period, the June 27, 1998 Ceyhan earthquake (M 6.2), that took place on the Misis-Ceyhan Fault (Aktar et al., 2000; Ergin et al., 2004), is considered as the largest event in the Adana Basin. The epicenter location and the source mechanism of this earthquake are well constrained by Aktar et al. (2000) providing clear evidence of pure left lateral strike-slip motion.

The 1408 earthquake (M 7.5) took place at the northern end of the DSFZ and is associated with ~20 km long surface rupture (Ambraseys & Melville 1995; Sbeinati et al. 2005; Akyüz et al. 2006). The 13 August 1822 (M 7.4) event was occurred in the Karasu Valley (Ambraseys 1989). Ambraseys (1989) reports that the 1872 April 3 earthquake (M 7.2) was occurred in the Amik Basin and generated heavy damage around the former Amik Lake. A destructive earthquake also took place in 1269 in the Adana Basin (Arvanitakis, 1903; Calvi, 1941; Guidoboni and Comastri, 2005), however, there is insufficient information in the literature to attribute this event to a specific fault segment.

Some moderate-size earthquakes (e.g. 1905, M 6.8 Malatya; 1971, M_s 6.7 Bingöl; 1986, M_s 6.0 Sürgü; 2003, M_s 6.4 Bingöl; 2010, M 6.0 Karakoçan–Elazığ; 2020, M 6.8 Elazığ) were occurred on the main trace of the EAFZ during the instrumental period (Tan et al., 2008) but no surface rupture was reported. It is noteworthy to note that the north-eastern part of the EAFZ reactivated with moderate size earthquakes during the instrumental period (Figure 3).

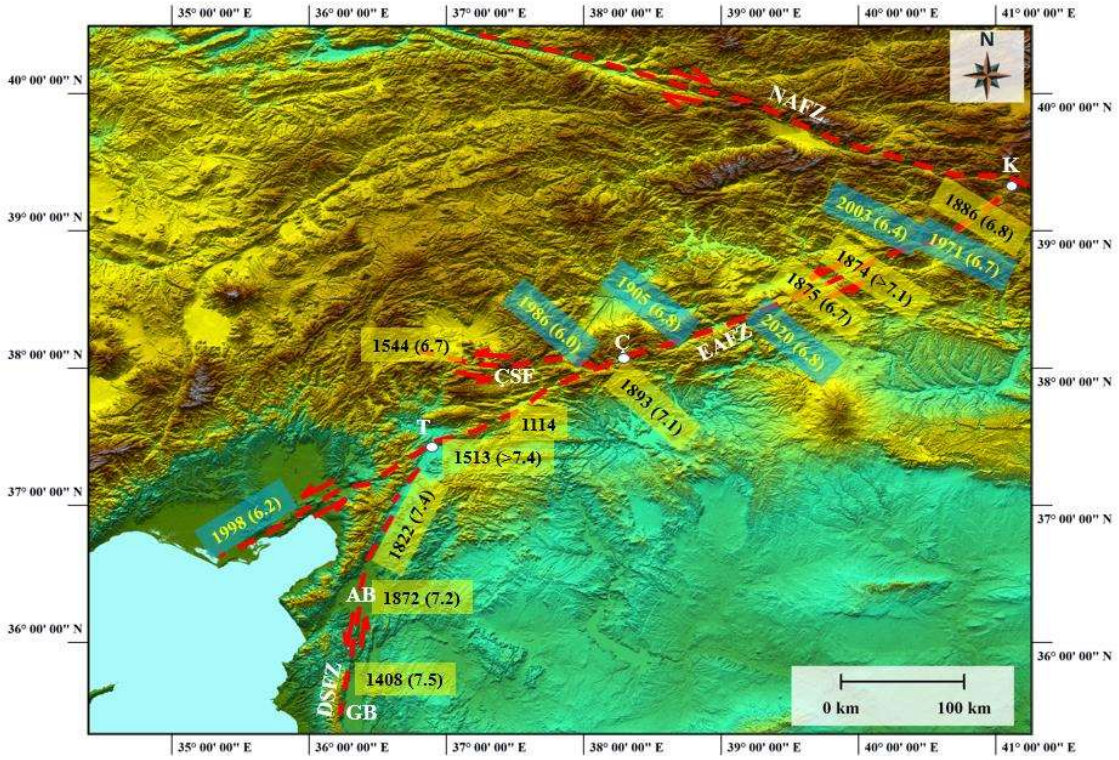

Figure 3. Instrumental (blue boxes with yellow numbers) and pre-instrumental (yellow boxes with black numbers) earthquake activity of the main trace of the EAFZ and northern DSFZ. NAFZ: North Anatolian Fault Zone, EAFZ: East Anatolian Fault Zone, DSFZ: Dead Sea Fault Zone, ÇSF: Çardak-Sürgü Fault, K: Karlıova, T: Türkoğlu, Ç: Çelikhan, AB: Amik Basin, GB: Ghab Basin. Map produced from SRTM Worldwide Elevation Data (1-arc-second resolution).

The southwestern parts of the EAFZ were reactivated during the February 6, 2023 earthquakes. Epicentral locations of mainshok and afterschok activity (Figure 4) show that the Narlı Segment and East Anatolian Fault are reactivated during the first event (M_w 7.8) and the Çardak Fault is reactivated during the second event (M 7.7). Preliminary field observations indicate the existence of surface ruptures along the Çardak Fault (personal communication with Dr. Taylan Sancar, Munzur University), Narlı Segment and East Anatolian Fault from Amik Basin in south to Çelikhan in northeast (Figure 5). It is difficult to determine the surface rupture properties (length of the rupture, dip of the fault plane, maximum displacement) without having comprehensive field observations and mapping. However, preliminary field observations suggest that the maximum horizontal

displacement is ~2.5 m on the Narlı Segment, ~4 m in south of Türkoğlu, and more than 5 m northeast of Türkoğlu (personal communication with Prof. Serdar Akyüz, ITU). The maximum horizontal displacement is ~ 6.7 m on the Çardak Fault (personal communication with Dr. Taylan Sancar, Munzur University).

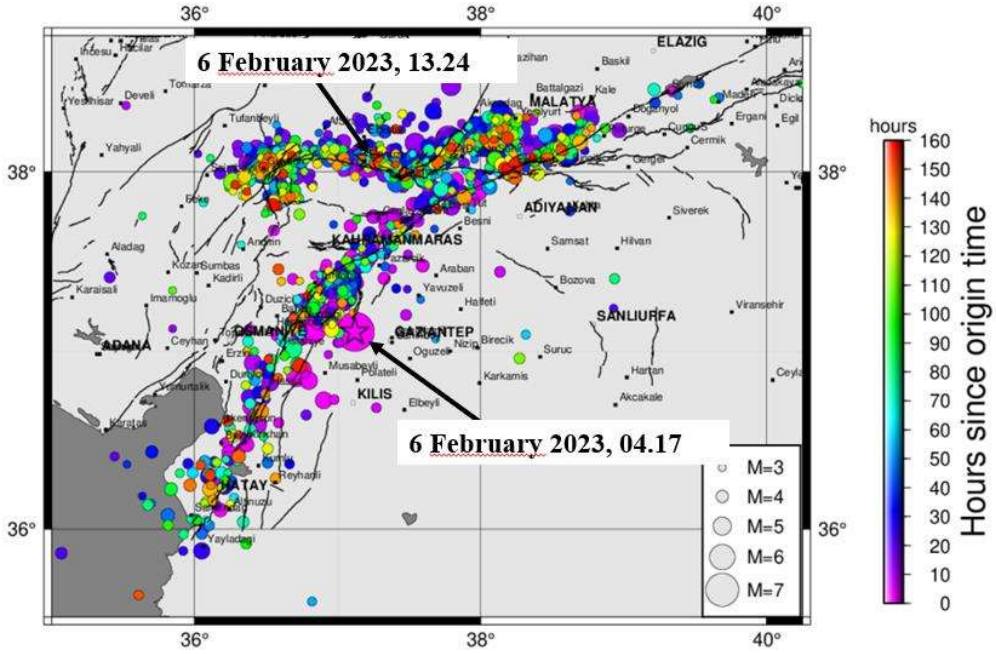

Figure 4. Epicenters of main shocks (stars indicated by black arrows) and aftershock activity of the 6 February 2023 earthquakes (Source: Kandilli Observatory and Earthquake Research Institution).

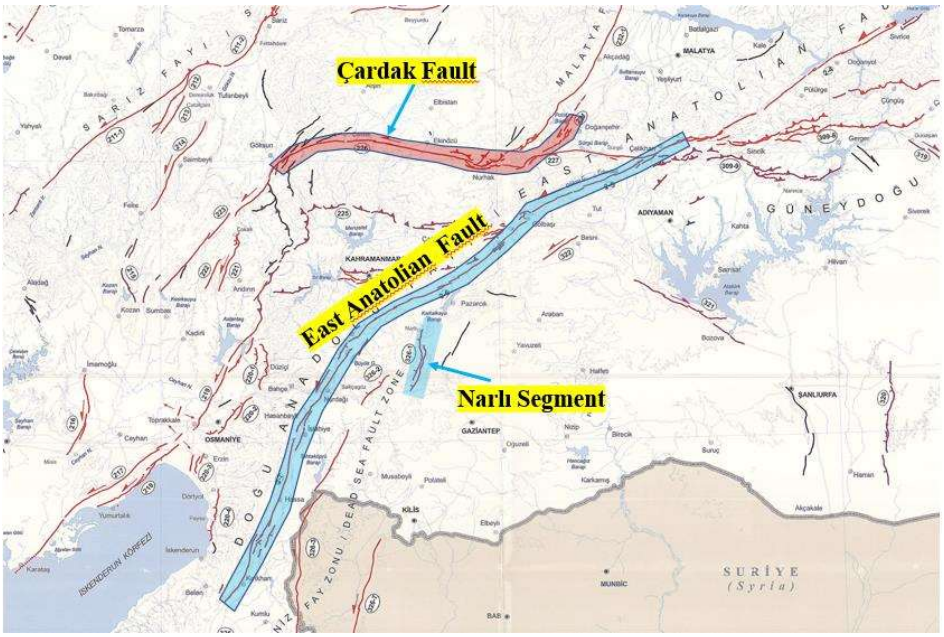

Figure 5. Reactivated faults during the February 6, 2023 earthquakes. Faults indicated with light blue colors were reactivated at 04.17 and fault with light color was reactivated at 13.24 (Emre et al. 2013).

3. SEISMIC ASPECTS

3.1. Deformation Rate

Crustal deformation rate is considered as a direct quantitative measure of seismic hazard. In general, the size of the earthquakes is larger and their frequency increases at regions of high deformation rate (strain rate). Seismological data (historical and instrumental period earthquake catalogues), geological field observations (offsets on the faults) and the GPS observations provide data for the assessment of deformation rates.

Palano et al., (2017) published a significant GPS data set established by reprocessing the available GPS data acquired in the region. For this report, adopting the Shen et al. (2015) algorithm, the GPS data are interpolated to get slip rates at equally spaced grid points. Then, a strain rate tensor is estimated at each grid point to understand spatial deformation pattern in the surroundings of the source region of the two major earthquakes. Following the strain rate tensor estimation, the second invariant strain rates shown in Figure 6, the post-1900 instrumental seismicity shown in Figure 7, and the MTA active faults (Emre et al., 2013) are considered for this assessment.

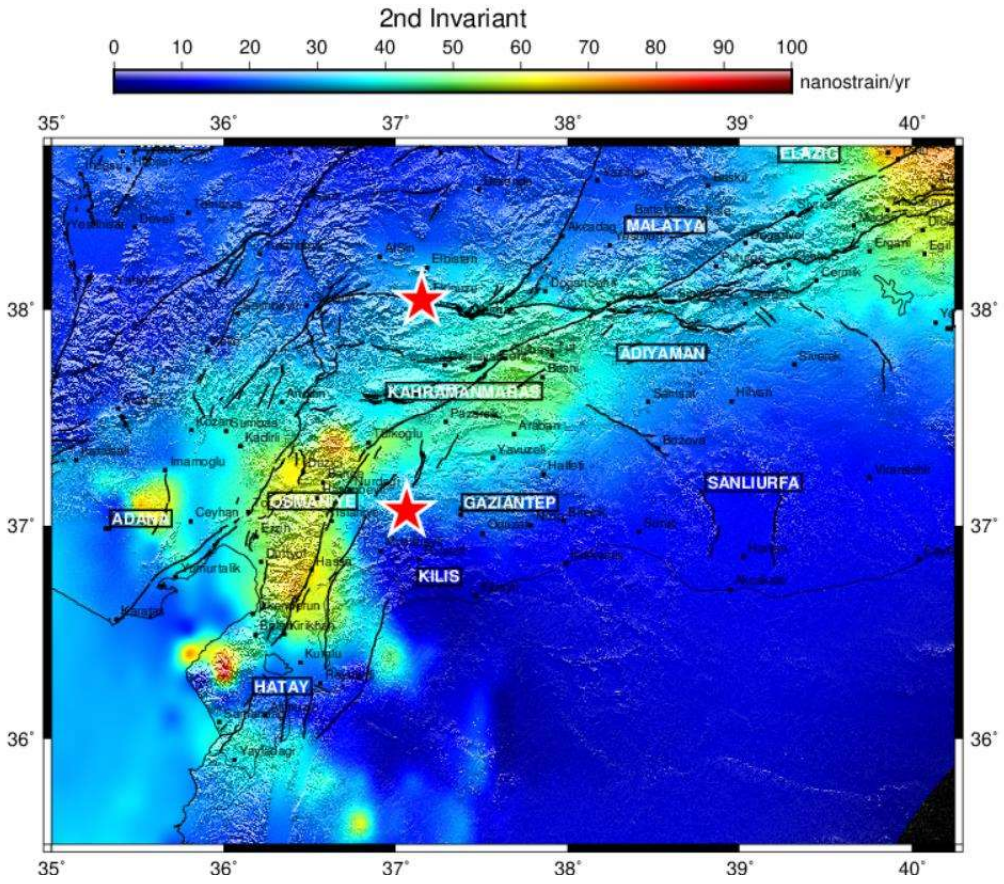

Figure 6. Spatial variation of second invariant strain rates around the EAFZ (EAFZ). The red stars indicate the epicenters of the February 6, 2023 major events.

It is obvious from strain rates shown in Figure 6 that the high deformation rates are associated around the main trace of the EAFZ and secondary fault branches occur around the main trace such as the Narlı fault where the February 6 rupture initiated or the Çardak fault that accommodated the second major event of moment magnitude M_w 7.7. We also observe relatively large strain rates around Osmaniye in Figure 6. The large strain rate region is bordered by distinct fault lines to the east and west of Osmaniye. Both EAFZ and Çardak fault can be considered as locked faults accumulating strain. This is based on the fact that they both represent a boundary between high and low-strain rate regions. The lack of seismicity along the NS trending fault occurring to the east of Osmaniye is noticeable portraying an ongoing strain accumulation. Although we know that this fault is one of the segments ruptured by the February 6, 04:17 earthquake (M_w 7.8), the observed seismicity along the western border fault line points out that this fault line may not be wholly locked.

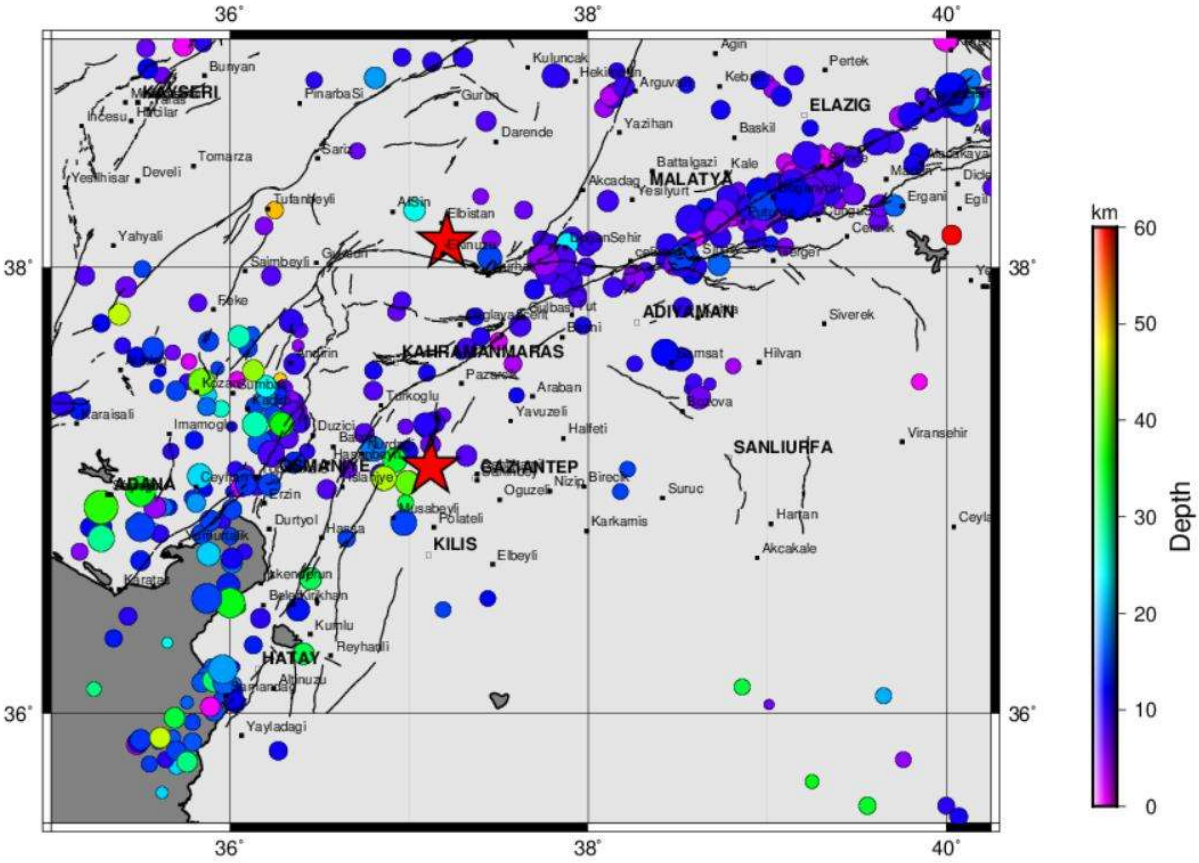

Figure 7. Seismicity of the region showing the location of the earthquakes (M > 4.0) from 1900 to March 2021. The International Seismological Center (ISC) reviewed well-constrained events are shown. The red starts represent the epicenters of M_w 7.8 and M_w 7.7 events.

Another striking point observed from the seismicity (Figure 7) and strain rate (Figure 6) maps is the footprints of the M_w 7.7 earthquake ruptured on February 6 at 13:24. No events of magnitude M > 4.0 are observed along the fault segment ruptured by the M_w 7.7 event from 1900 to March 2021 (end of the ISC -International Seismological Center- reviewed catalog period). Similarly, one can distinguish the lack of seismicity along the fault segment to the northeast of the epicenter of the 04:17 event. That fault segment experienced a major coseismic moment release during the first major (M_w 7.8) earthquake.

3.2. Source Rupture Characteristics of the February 6, 2023 Earthquakes

The source regions of the two earthquakes are clearly depicted by the aftershock distribution located by Kandilli Observatory and Earthquake Research Institute (KOERI). The aftershock distribution in Figure 4 points out the source extent of the first and second major earthquakes denoting ~300 km and ~150 km long rupture length (Figure 5). The locations of the rupture initiation of the two events are also shown in Figure 5. It is quite obvious from the aftershock distribution that the northeast rupture extent of the first event terminated in the proximity of the source area of the second event that ruptured approximately nine hours later.

The curvature in the aftershock distribution associated with the M_w 7.8 event (at 04:17) suggests a bilateral rupture on different segments oriented (a) NE-SW in the northeast area of the rupture zone and (b) striking NNE-SSW in the southern section toward the city of Antakya (Antioch) in Hatay province. The rupture complexity of this event is also observed at the strong motion station located approximately 30 km away from the epicenter towards NE (Figure 8) and from a slip distribution model obtained through modeling of the tele-seismic body waves using the algorithm of Kikuchi et al. (1991). One can easily depict three distinct pulses, which are visible in the displacement seismograms. The narrow nature of the first pulse suggests a rupture propagation towards the strong-motion station while the second pulse points a rupture propagation outwards the strong-motion station towards southwest along a fault line portrayed by the aftershock distributions given in Figure 4.

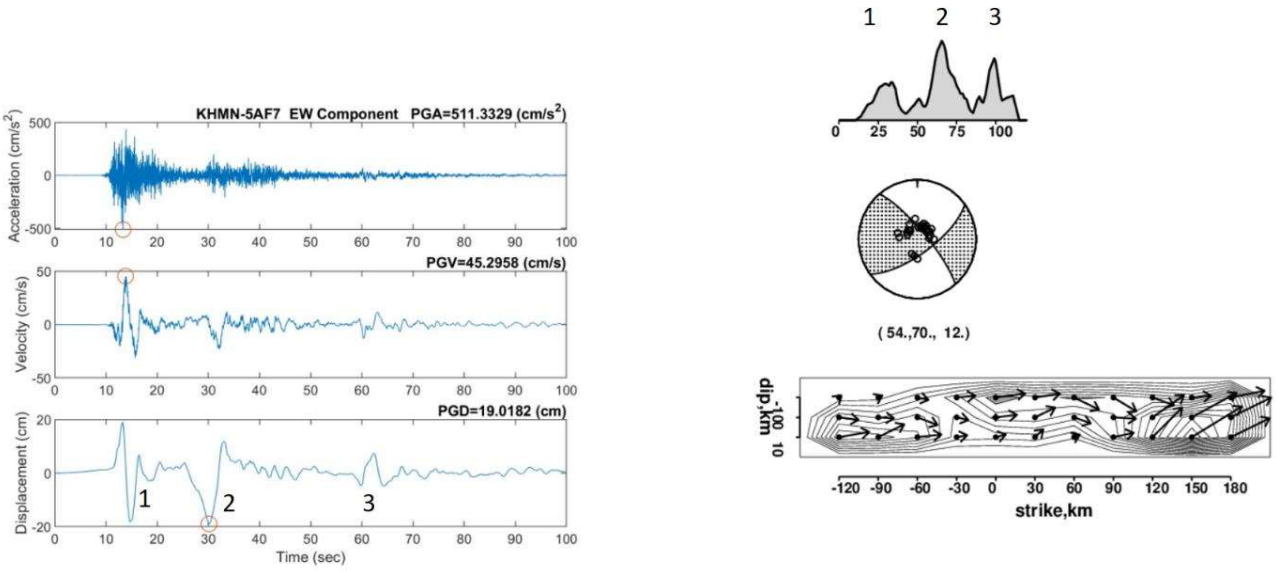

Figure 8. Rupture complexity of the February 6, 04:47 earthquake (M_w 7.8) observed at the seismograms recorded at the KOERI strong motion station located in Kahramanmaraş. The three distinct pulses (labeled on the plots) point out ruptures on different fault segments. Coseismic rupture on different fault segments associated with the mainshock is also derived from the modeling of the teleseismic body waves using the inversion method of Kikuchi et al. (1991). The negative distances are toward the northeast and the positive distances extend toward the southwest. The moment rate function on top of the right panel and the slip model in the lower right panel depicts ruptures on four segments.

A large seismic phase is noticeable in the later portion of the seismograms shown in Figure 9. Such a later arrival could reflect either a fault rupture or a phase generated at an interface. Modeling this phase as a fault rupture yields a long moment rate function denoting a rupture time of about 80 seconds. The waveforms recorded at the Matsushiro station (MAJO) are selected to show the extraordinarily long rupture time (Figure 9). Since the distance of the MAJO station to the 04:17 and 13:24 earthquake epicenters is almost identical, the lack of later phase arrival in the 13:24 seismogram suggests that the pulse in the 04:17 is associated with a fault rupture.

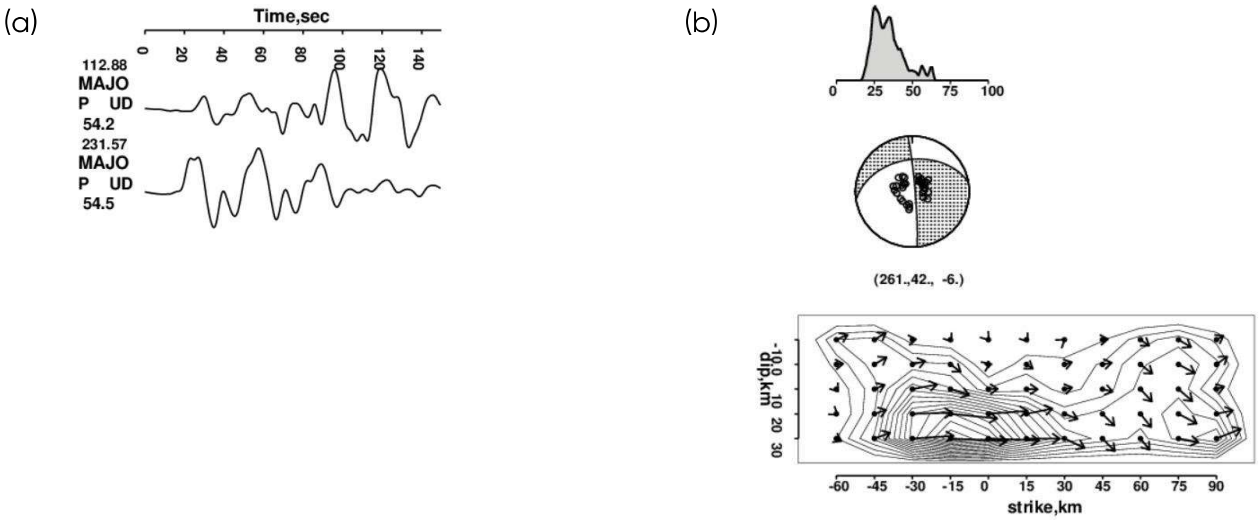

Figure 9. (a) The seismograms generated by the 04:17 (top) and 13:24 (bottom) earthquakes were recorded at MAJO station. (b) A finite source model for the 13:24 event (M_w 7.7). The negative distances extend toward the east and the positive distances toward the west.

Despite the magnitude of the 13:24 event (M_w 7.7) is very close to the size of the 04:17 earthquake, the waveform modeling of the tele-seismic body waves points out rather a simple rupture pattern (Figure 9b). The rake angles derived at each grid point denote strike-slip faulting. Slight compression and extension component are developed at the eastern and western sections of the source area. This fact is also observed from the focal mechanisms of the aftershocks reported by the European Mediterranean Seismological Center (EMSC).

4. EARTHQUAKE TRIGGERING

A rupture or a movement on a fault causes stress changes on nearby faults by releasing the stress that had been accumulating. Depending on the faulting mechanism and the regional stress tensor orientation, Coulomb stress increases at certain regions while decreases in some other locations. Such an interaction between fault ruptures is known as earthquake triggering via Coulomb Failure Stress Changes. Triggering of an earthquake by stress increase was observed in several regions (King et al., 1994; Stein et al., 2002; Hardebeck and Okada, 2018).

Most of the aftershocks tend to occur at regions of increased stresses. Their spatial distribution is well explained by Coulomb failure criterion (King et al., 1994; Harris et al, 2002). The magnitude of the strongest aftershock usually is one unit below the magnitude of the mainshock. The aftershocks take place on the ruptured fault plane and its nearby vicinity. There are several definitions of aftershocks. For example, earthquakes of certain magnitudes occurring within a

certain time-and spatial-extent of the mainshock epicenter are classified as aftershocks (Table 3).

Table 3. Aftershock classification according to magnitude, distance from the mainshock area and time elapsed since the mainshock origin time (Gardner and Knopoff, 1974).

M	L(km)	T(days)
2.5	19.5	6
3.0	22.5	11.5
3.5	26	22
4.0	30	42
4.5	35	83
5.0	40	155
5.5	47	290
6.0	54	510
6.5	61	790
7.0	70	915
7.5	81	960
8.0	94.0	985

As per the definition of Gardner and Knopoff (1974) it is a matter of debate to consider the M_w 7.7 event, that took place on February 6, 2023 at 13:24 local time, as an aftershock of the M_w 7.8 earthquake. If only the distance between the ruptured segments of these two events is considered, which is less than 81 km, the second event (M_w 7.7) can be regarded as the aftershock of the M_w 7.8 event according to Table 3. However, the declustering method (classification of earthquakes as aftershocks and mainshocks -i.e., dependent vs. independent events) proposed by Gardner and Knopoff (1974) classify the M_w 7.8 and M_w 7.7 earthquakes as independent because the distance between the epicenters of these two events is larger than 81 km (Table 3).

The triggering of earthquakes on nearby faults happen in different time frames. It could be in the order of seconds, minutes, hours, days, months or even in a couple of years. For example, it was approximately three months for the November 12, 1999 Düzce earthquake (M_w 7.2) to be triggered by the August 17, 1999 Izmit earthquake (M_w 7.5). Triggering between the February 6, 2023 major events happened in about nine hours. That is, the second event (M_w 7.7) was triggered after the occurrence of the first event (M_w 7.8) with a difference of 9 hours.

Another very good example of earthquake triggering case is observed within the first major event (M_w 7.8) of the February 6, 2023 earthquake sequence. The aftershock distributions, waveform modelling, coseismic surface ruptures observed by field geologists, and satellite images point out that the mainshock was associated with multiple ruptures on several fault segments. That is, multiple triggering earthquakes occurred within a couple of seconds in the February 6, 2023 M_w 7.8

mainshock and consequently the rupture process time of the M_w 7.8 earthquake inferred from the waveform modelling of the teleseismic waveforms is more than 80 seconds (Figure 9).

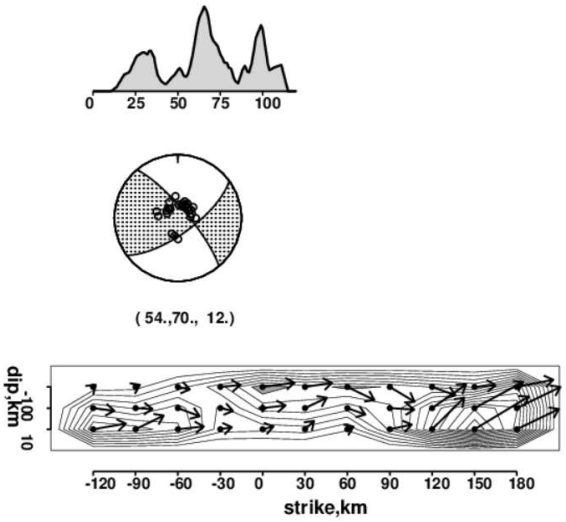

Figure 9. A rupture modelling for the February 6, 2023 04:17 earthquake (Mw7.8) using teleseismic body waves.

5. COULOMB STRESS CHANGE MODELING

Coulomb stress changes associated with the M_w 7.8 event and a possible triggering interaction between the M_w 7.8 and M_w 7.7 events were investigated by Toda et al. (2023) identifying stress enhancement on the M_w 7.7 fault rupture plane. The modelling by Toda et al. (2023) is based on focal mechanism solution and finite source model of USGS released on February 6 soon after the mainshock. The authors estimated about one bar stress increase on the fault ruptured by the M_w 7.7 event and about 3-5 bars stress increase on the tips of the ruptured EAFZ fault segments. Toda et al. (2023) also identified a stress decrease region in the area between the fault planes ruptured by the M_w 7.8 and M_w 7.7 earthquakes (i.e. between the EAFZ and the Sürgü-Çardak fault) as presented in Figure 10.

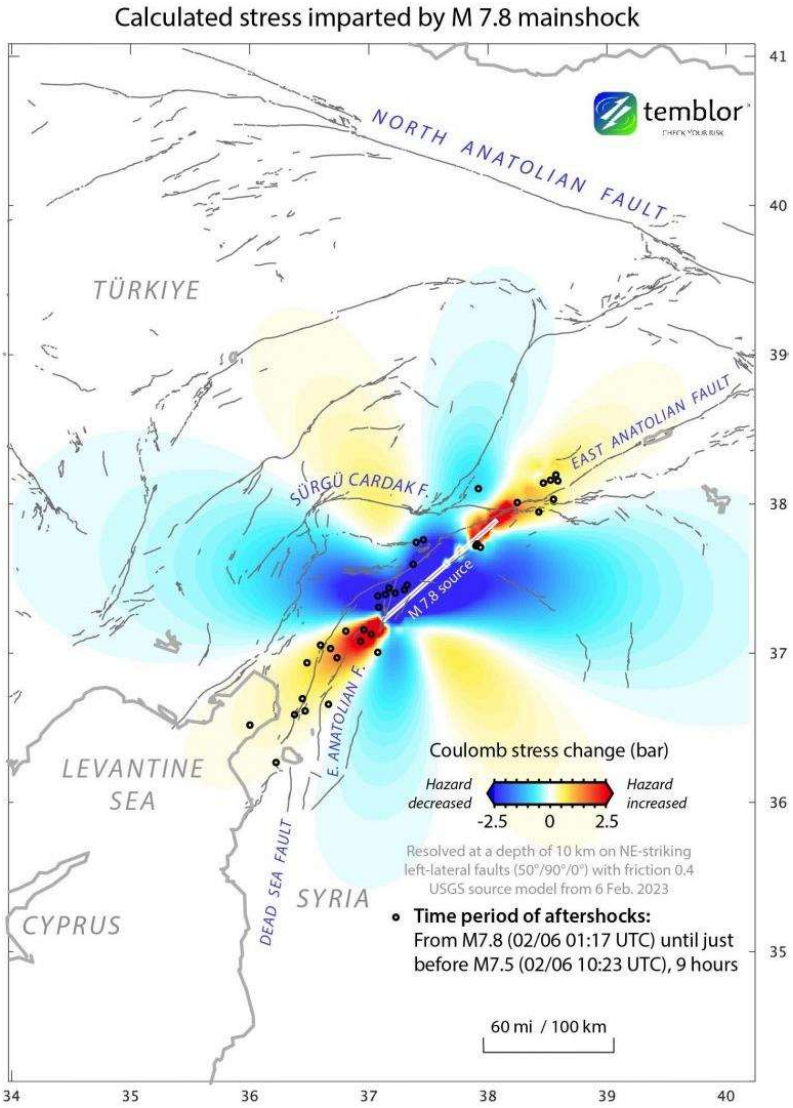

Figure 10. Coulomb stress changes associated with the M_w 7.8 event (Toda et al., 2023).

It should be noted that despite a stress increase on the Çardak fault as reported by Toda et al. (2023) due to M_w 7.8 event, no seismic activity was reported by Kandilli Observatory and Earthquake Research Institute (KOERI). The only reported event is the M 3.8 foreshock occurred about three hours (10:26 local time) before the M_w 7.7 event that was located at latitude 38.14N, longitude 37.45E close to the epicenter (Figure 11).

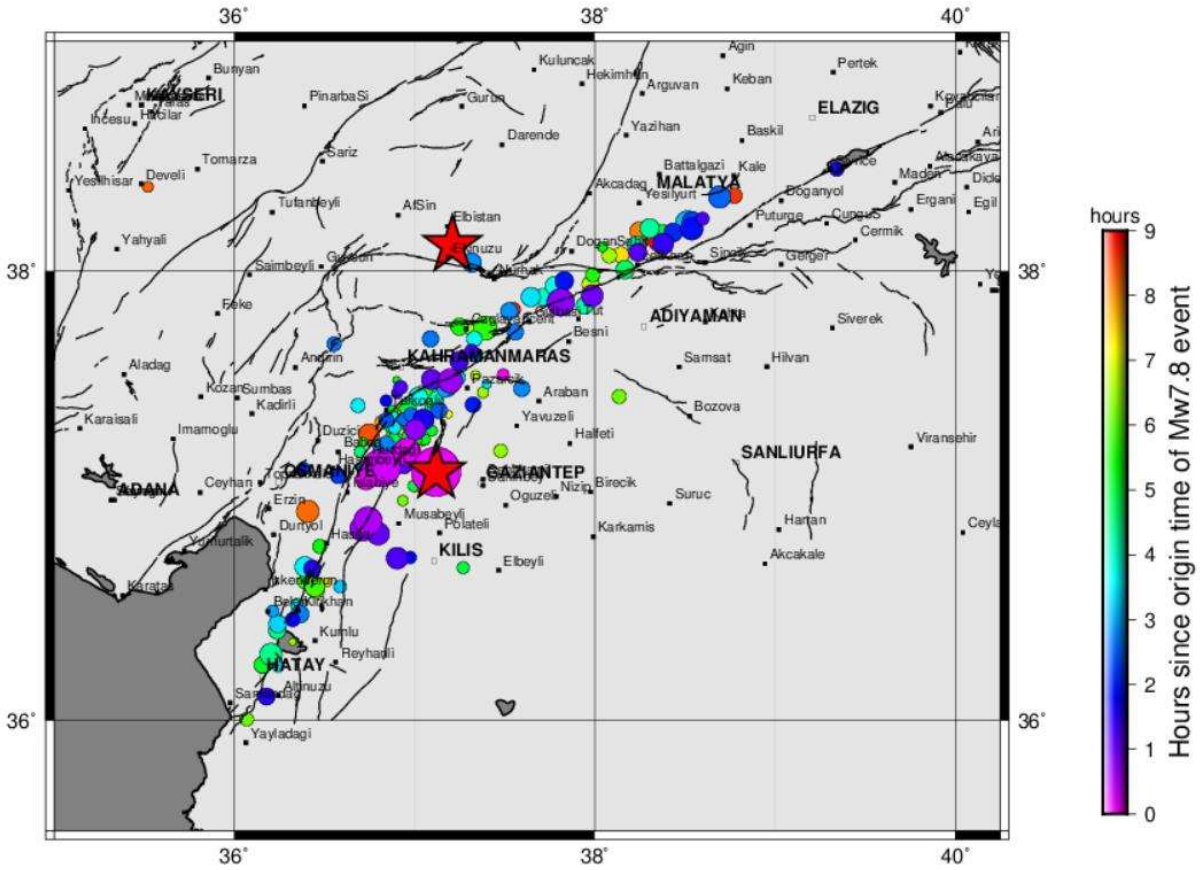

Figure 11. Aftershock distribution of the events occurred prior the M_w 7.7 earthquake

The Coulomb stress change modelling of Toda et al. (2023) is based on USGS focal mechanism solution (https://earthquake.usgs.gov/earthquakes/eventpage/us6000jllz/executive) and finite source model determined immediately after the M_w 7.8 event. An alternative Coulomb stress change model is developed for this report using a different finite source model based on the GCMT focal mechanism parameters (https://www.globalcmt.org/cgi-bin/globalcmt-cgi-bin/CMT5/form?itype=ymd&yr=2023&mo=2&day=6&oyr=1976&omo=1&oday=1&jyr=1976&jday=1&ojyr=1976&ojday=1&otype=nd&nday=1&lmw=0&umw=10&lms=0&ums=10&lmb=0&umb=10&llat=-90&ulat=90&llon=-180&ulon=180&lhd=0&uhd=1000&lts=-9999&uts=9999&lpe1=0&upe1=90&lpe2=0&upe2=90&list=0). The major difference between the USGS and GCMT fault plane solutions is the dip of the fault plane; GCMT reports a dip angle of 70 degrees, SE dipping fault plane while the dip angle of the USGS solution is reported as 88 degrees, dipping NW. The difference between the two focal mechanisms is significant and differences in fault slip models significantly affect the Coulomb stress change results. We develop a slip model to use in Coulomb stress change calculations based on the faulting parameters of GCMT solutions.

Using the teleseismic body waves, the satellite images of the source region and the aftershock distributions we constructed a grid scheme that is 300 km long along the strike and extending 20 km along the dip of the fault plane. The gridding size is selected as 30 km along strike and 10 km along dip. The waveform fitting between the observed and calculated seismograms was achieved by trial and error by adjusting the rupture velocity, rise time, window number, and smoothing parameters. The resulting slip distribution model is shown in Figure 12. The arrows in the model indicate the rake angle at the grid points. The horizontal arrows correspond to strike parallel faulting. The downward and upward bias of the arrows from horizontal shows transtention and transpression, respectively. The transpressional features in the NE side of the slip model corresponds to the well-known Çelikhan restraining bend where the rupture stopped.

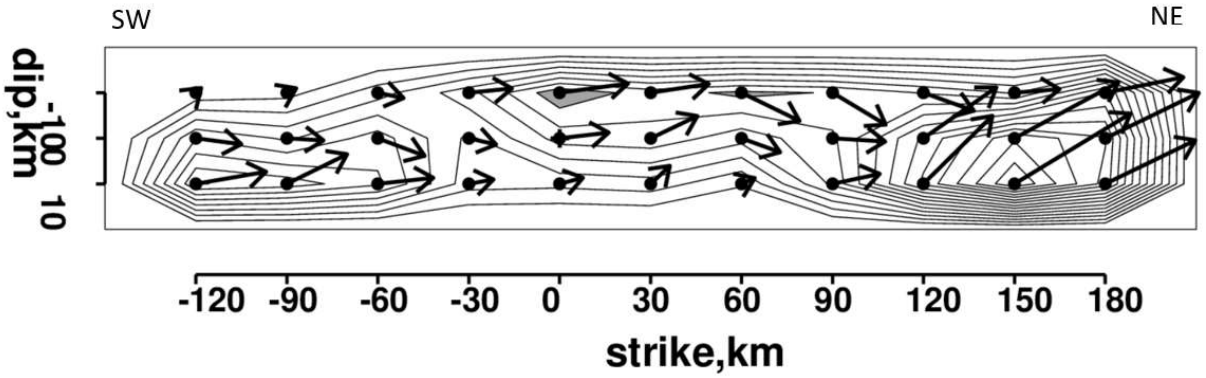

Figure 12. A fault slip model for the M_w7.8 earthquake. The NE termination locus of the rupture is in the proximity to Çelikhan restraining bend.

The Coulomb stress change calculations are done using the software developed by the authors of Toda et al. (2023). We used the same input parameters that were used by Toda et al. (2023) except the variable slip distribution model developed in this study. Using the inferred rake angles at each grid point the slip values are resolved into strike-slip and dip-slip components. The upward motion direction is NW. Thus, significant reverse faulting motion toward NW contributes to the Coulomb stress change calculations. Considering the proximity of the NE part of the slip model to the eastward extent of the Çardak fault, one would expect a significant difference between our results with those derived by Toda et al. (2023).

The Coulomb stress change model estimated in this study is illustrated in Figure 13. The EAFZ accommodates the motion between Anatolian Block and the Arabian Plate. The Çardak fault is located in the Anatolian Block. Therefore, we are especially interested in stress changes in the Anatolian Block associated with the M_w 7.8 event. A stress decrease region close to Kahramanmaraş and stress increase region close to Çardak fault are two distinct features of the

Coulomb model (Figure 13). In the stress decrease region close to the releasing band to the east of Kahramanmaraş transtensional motion would be expected that is confirmed by a large aftershock showing predominantly normal faulting (Figure 14). Essentially, the Coulomb stress change calculation results given in Figure 13 show a significant stress increase in the eastern part of the Çardak fault that probably brought the fault to failure.

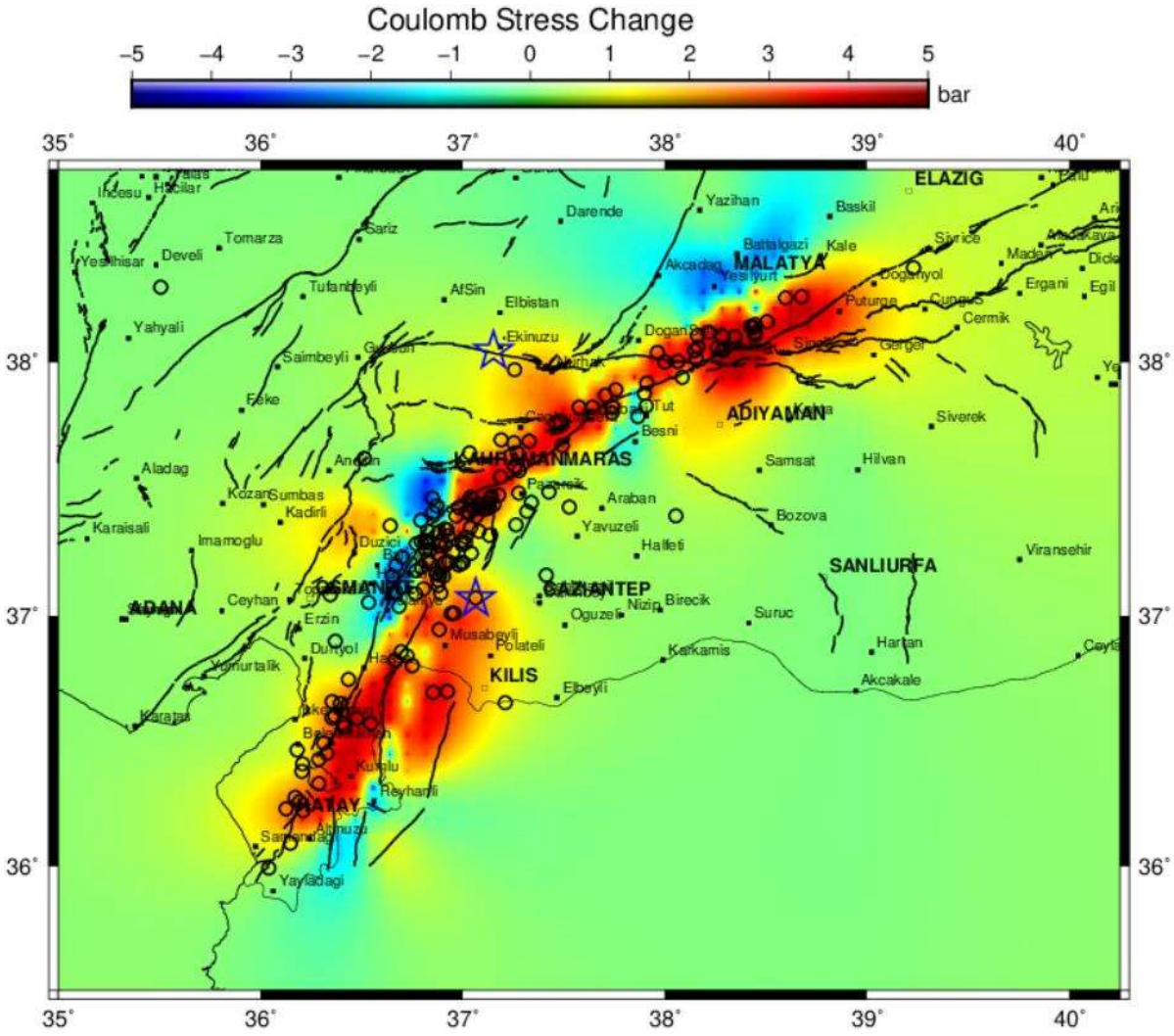

Figure 13. Stress changes associated with the February 6, 04:17 earthquake (M_w7.8)

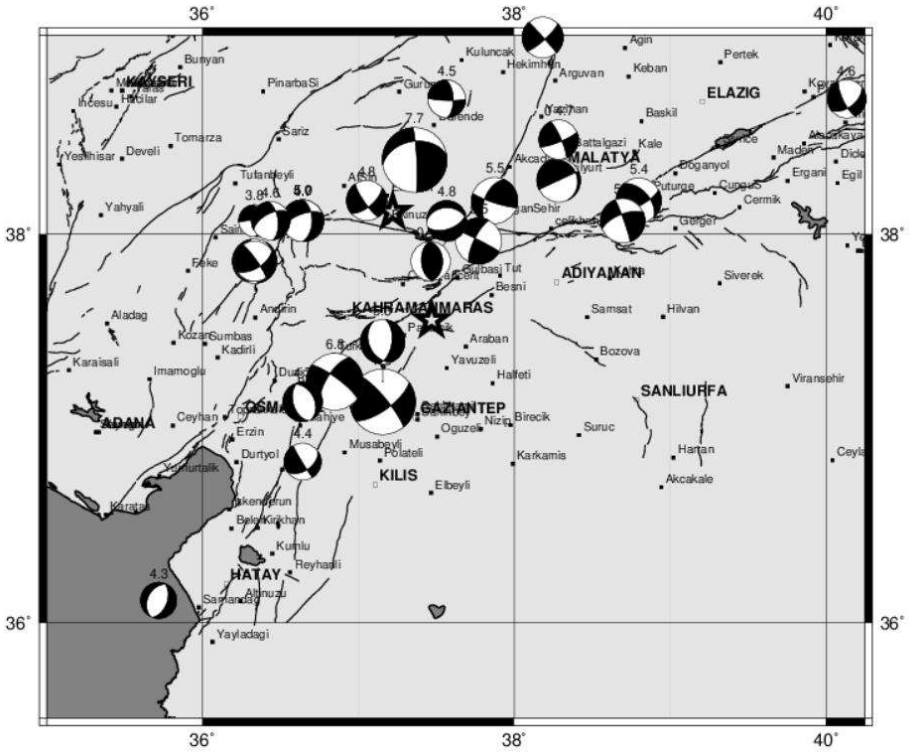

Figure 14. Focal mechanism of the aftershocks of the February 6, 2023 earthquakes.

6. CONCLUSIONS

Several fault segments in the EAFZ were reactivated during the February 6, 2023 earthquakes. Current geological observations and seismic data indicate that the main branch of the EAFZ was ruptured between Amik Basin in the south and Celikhan in the north during the M_w 7.8 (first) earthquake at 04:17, local time. The second earthquake with M_w 7.7 at 13:24 occurred on the western part of the Sürgü-Çardak Fault, which splits from the East Anatolian Fault. The faults that caused the February 6, 2023 events are shallow active faults that were also associated with large earthquakes in the historical periods.

The objective of this report is to understand whether Coulomb failure stress changes associated with the M_w 7.8 earthquake fault ruptures brought the Sürgü-Çardak fault to failure with a M_w 7.7 earthquake, nine hours after the M_w 7.8 event. A detailed fault slip model for the M_w 7.8 mainshock was established by modeling the waveforms generated by multiple fault segment ruptures. The resulting finite source model indicates transtension and transpression in the proximity of known releasing and restraining regions along the EAF zone.

Kanamori and Anderson (1975) reported stress drops associated with large interplate and intraplate earthquakes and determined an average static stress drop of 60 bars. The authors also determined the following relation between static stress drop ($\Delta\sigma$) and seismic moment (Mo),

$$\Delta\sigma = \frac{Mo}{2.5S^{1.5}}$$

where S is the source area. The GCMT seismic moment for the 13:24 event is reported as ≈5.0x10^{27} dyn·cm. The USGS seismic moment is 5.05 x10^{27} dyn·cm that is very close to GCMT seismic moment (https://earthquake.usgs.gov/earthquakes/eventpage/us6000jlqa/finite-fault). The finite source model of USGS shows that the major moment release took place on a fault area of 80 km x 20 km. This in turn, yields a stress drop estimate of $\Delta\sigma \approx 30\ bars$ for the major asperity ruptured by the 13:24 event.

The restraining bend in the NE end of the ruptured fault plane during the first earthquake plays a significant role in Coulomb stress changes, which results in stress increase in the eastern part of the Sürgü-Çardak fault. The Coulomb stress enhancements on the Sürgü-Çardak fault decrease to ~1 bar in the hypocenter in the westward direction (Figure 13). If we assume a $\Delta\sigma$ accumulation of 30 bars on the Sürgü-Çardak fault since the previous seismic moment release, then we can make an approximate calculation for the stress accumulation rate on the same fault. Sesetyan et al. (2023) reported the 1544 earthquake (M_w 7.0 ± 0.75) as the previous major event on the Sürgü-Çardak fault. The plaseoseismological data, on the other hand, suggest that the previous major event on the Sürgü-Çardak fault occurred in 500 AD. The 1544 historical earthquake as stated by Sesetyan et al. (2023) or the event occurred in 500 AD according to the paleoseismological data yield a stress rate of approximately 0.06 bars/yr and 0.02 bars/yr, respectively. Thus, the 1 bar Coulomb stress increase in the hypocentral area suggests that the M_w 7.7 event should have occurred at a later time depending on the stress accumulation rate, which seems to range between 0.02 to 0.06 bars/yr. That is, if one considers 30 bars bearing capacity and no interaction between the M_w 7.8 and M_w 7.7 events, then the Çardak Fault would have been ruptured in the order of years. Of course, we are aware of the fact that the uncertainties in providing such a punctual estimate is quite high.

In brief, the M_w 7.8 event that occurred at 04:17 transferred additional stress on the eastern part of the Sürgü-Çardak fault, that initiated the rupturing of the M_w 7.7 event, which might have occurred many years later if such stress transfer has not taken place.

REFERENCES

Aktar, M.T., Yörük, A., Kaplan, H., 1994. Kurtkulağı events in the Cilician Basin and its aftershocks. In: XXIV General Assembly of the European Seismological Com-mission, Proceedings and Activity Report, Athens, vol. 1, pp.74–80.

Aktar, M., Ergin, M., Özalaybey, S., Tapirdamaz, C., 2000. A lower-crustal event in the northeastern Mediterranean: the 1998 Adana Earthquake (Mw:6.2) and its aftershocks. Geophys. Res. Lett.27, 2361–2364.

Akyüz, S.H., Altunel, E., Karabacak, V., Yalçıner, C.C., 2006. Historical earthquake ac-tivity of the northern part of the Dead Sea Fault Zone, southern Turkey. Tectono-physics426, 281–293.

Allen, C.R., 1969. Active Faulting in Northern Turkey. Contr. 1577. Div. Geol. Sciences, Calif. Inst. Tech., p.32.

Altunel, E., Meghraoui, M., Karabacak, V., Akyüz, S., Ferry, M., Yalçıner, Ç., Munschy, M., 2009. Archaeological sites (Tell and Road) offset by the Dead Sea Fault in the Amik Basin, Southern Turkey. Geophys. J. Int.179, 1313–1329. http://dx.doi.org/10.1111/j.1365-246X.2009.04388.x.

Ambraseys, N.N., 1989. Temporary seismic, quiescence: SE Turkey. Geophys. J.96, 311–331.

Ambraseys, N.N. & Melville, C.P., 1995. Historical evidence of faulting in eastern Anatolia and northern Syria, Ann. Geophys. 38(3–4), 337–343.

Arpat, E., ¸Saroğlu, F., 1975. Türkiye'deki bazı önemli genç tektonik olaylar. TJK Bül.18, 91–101.

Arvanitakis, G.L., 1903. Essai d'une statistique des templements de terre en Palestineet Syrie. Bull. Inst. Egypte4 (4), 178–183.

Barka, A., Kadinsky-Cade, K., 1988. Strike-slip fault geometry in Turkey and its in-fluence on earthquake activity. Tectonics7 (3), 663–684.

Barka, A., Reilinger, R., 1997. Active tectonics of the Mediterranean region: deduced from GPS, neotectonic and seismicity data. Ann. Geofis.XI (3), 587–609.

Calvi, S., 1941. Türkiye ve bazı komşu ülkelerin deprem kataloğu, Çeviren: Erdoğan Kumcu, 1979. 'Istanbul.

Chorowicz, J., Luxey, P., Lyberis, N., Carvalho, J., Pairot, J.F., Yürür, T., Gündoğdu, N., 1994. The Maraş Triple junction (Southern Turkey) based on digital ele-vation model and satellite imagery interpretation. J. Geophys. Res.99 (B10), 20225–20242.

Dewey, J.F., Pitman, W.C. III, Ryan, W.B.F., Bonnin, J., 1973. Plate tectonics and the evolution of the Alpine System. Geol. Soc. Am. Bull.84, 3137–3180.

Duman, T.Y., Emre, Ö., 2013. The East Anatolian Fault: geometry, segmentation and jog characteristics. Geol. Soc. (Lond.) Spec. Publ.372.

Emre, Ö., Duman, T.Y., Özalp, S., Elmacı, H., Olgun, Ş. ve Şaroğlu, F., 2013. Açıklamalı Türkiye Diri Fay Haritası. Maden Tetkik ve Arama Genel Müdürlüğü, Özel Yayın Serisi-30. Ankara-Türkiye.

Ergin, M., Aktar, M., Eyidoğan, H., 2004. Present-day seismicity and seismotectonics of the Cilician Basin: Eastern Mediterranean Region of Turkey. Bull. Seismol. Soc. Am.94, 930–939. http://dx.doi.org/10.1785/0120020153.

Gardner, J. K., and L. Knopoff (1974). Is the sequence of earthquakes in Southern California, with aftershocks removed, Poissonian?, Bull. Seis. Soc. Am., 64(5), 1363–1367

Guidoboni, E., Comastri, A., 2005. Catalogue of Earthquakes and Tsunamis in the Mediterranean Area from the 11th to the 15th Century. Istituto Nazionale di Geofisica e Vulcanologia.

Hardebeck, J. L., & Okada, T. (2018). Temporal stress changes caused by earthquakes: A review. Journal of Geophysical Research: Solid Earth, 123, 1350–1365. https://doi.org/10.1002/2017JB014617

Harris, R. A., Dolan, J. F., Hartleb, R., & Day, S. M. (2002). The 1999 Izmit, Turkey, earthquake: A 3D dynamic stress transfer model of intraearthquake triggering. Bulletin of the Seismological Society of America, 92(1), 245–255. https://doi.org/10.1785/0120000825

Hempton, M.R., 1987. Constraints on Arabian plate motion and extensional history of the Red Sea. Tectonics6, 687–705.

Jackson, J., McKenzie, D., 1984. Active tectonics of the Alpine–Himalayan belt be-tween western Turkey and Pakistan. Geophys. J. R. Astron. Soc.77, 185–264.

Jörg, W., 1986. Türkei: Die Südküste von Kaunos bis Issos. München Artemis-Verlag, Zürih. ISBN3-7608-0791-7.

Karabacak, V. 2007. Ölü Deniz Fay Zonu Kuzey Kesiminin Kuvaterner Aktivitesi (Quaternary Activity of the Northern Part of the Dead Sea Fault), Eskişehir Osmangazi Üniversitesi, Fen Bilimleri Enstitüsü.

Kelling, G., Gökçen, S.L., Floyd, P.A., Gökçen, N., 1987. Neogene tectonics and plate convergence in the Eastern Mediterranean: new data from southern Turkey. Ge-ology15, 425–429.
Kempler, D., Garfunkel, Z., 1991. Northeast Mediterranean triple junction from a plate kinematics point of view. Bull. Tech. Univ. Istanb.44, 425–454. Spec. Is-sue.
Kikuchi, M., and Kanamori, H., 1991. Inversion of complex body waves-III, Bull. Seism. Soc.Am., 81, 2335-2350.
King, G. C., Stein, R. S., & Lin, J. (1994). Static stress changes and the triggering of earthquakes. Bulletin of the Seismological Society of America, 84(3), 935–953.
Koçyiğit, A., Erol, O., 2001. A tectonic escape structure: Erciyes pull-apart basin, Kay-seri, central Anatolia, Turkey. Geodin. Acta14 (2001), 133–145.
Lovelock, P.E.R., 1984. A review of the tectonics of the northern Middle East region. Geol. Mag.121 (6), 577–587.
Lyberis, N., Tekin, Y., Chorowicz, J., Kasapoğlu, E., Gündoğdu, N., 1992. The East Anatolian Fault: an oblique collisional belt. Tectonophysics 204, 1–15.
McClusky, S.C., Balassanian, S., Barka, A., Ergintav, S., Georgie, I., Gurkan, O.,Hamburger, M., Hurst, K., Kahle, H., Kastens, K., Kekelidse, G., King, R., Kotzev, V., Lenk, .,Mahmout, S., Mishin, A., Nadaria, M., Ouzounis, A., Paradisissis, D., Peter, Y., Pirilepin, M., Reilinger, R.E., Sanli, I., Seeger, H., Teableb, A., Toksöz, N., Veis, V., 2000. Global Positioning System constraints on plate kinematics and dynamics in the eastern Mediterreanen Caucasus. Journal of Geophysical Research 105, 5695–5719.
McKenzie, D.P., 1970. Plate tectonics of the Mediterranean region. Nature220, 239–343.
McKenzie, D.P., 1972. Active tectonics of Mediterranean region. Geophys. J. R. Astron. Soc.30, 109–185.
McKenzie, D.P., 1976. The East Anatolian fault: a major structure in eastern Turkey. Earth Planet. Sci. Lett.29, 189–193.
Muehlberger, R.W., Gordon, M.B., 1987. Observations on the complexity of the East Anatolian Fault, Turkey. J. Struct. Geol.9, 899–903.
Över, S., Özden, S., Yılmaz, H., 2004. Late Cenozoic stress evolution along the Karasu Valley, SE Turkey. Tectonophysics380 (2004), 43–68.
Palano, M., 2015. On the present-day crustal stress, strain-rate fields and mantle anisotropy pattern of Italy, Geophys. J. Int., 200(2), 969–985.
Perinçek, D., Çemen, ˙I., 1990. The structural relationship between the East Anatolian and Dead Sea fault zones in southeastern Turkey. Tectonophysics172, 331–340.
Reilinger, R., McClusky, S., Vernant, P., Lawrence, S., Ergintav, S., Cakmak, R., Ozener, H., Kadirov, F., Guliev, I., Stepanyan, R., Nadariya, M., Hahubia, G., Mahmoud, S., Sakr, K., ArRajehi, A., Paradissis, D., Al-Aydrus, A., Prilepin, M., Guseva, T., Evren, E., Dmitrotsa, A., Filikov, S.V., Gomez, F., Al-Ghazzi, R., Karam, G., 2006. GPS constraints on continental deformation in the Africa–Arabia–Eurasia conti-nental collision zone and implications for the dynamics of plate interactions. J. Geophys. Res., Solid Earth111 (B5), B05411. 52 p.
Sbeinati, M.R., Darawcheh, R. & Mouty, M., 2005. The historical earthquakes of Syria; an analysis of large and moderate earthquakes from 1365 B.C. to 1900 A.D., Ann. Geophys., 48(3), 347–435.
Shen, Z.-K.,Wang, M., Zeng, Y. &Wang, F., 2015. Optimal interpolation of spatially discretized geodetic data, Bull. seism. Soc. Am., 105(4), 2117–2127.
Sieberg, A., 1932. Erdbebengeographie. In: Gutenberg, B. (Ed.), Handbuch der Geo-physik, vol. 4, pp.775–812. Berlin.
Soysal, H., Sipahioğlu, S., Kolçak, D., Altınok, Y., 1981. Türkiye ve Çevresinin Deprem Katalogu, MÖ 2100-MS 1900 (Earthquake Catalogue of Turkey and Surroundings, BC 2100-AD 1900). TÜB˙ITAK Project (No. TBAG 341), 99 s.
Şaroğlu, F., Emre, Ö., Kuşçu, I., 1992. The East Anatolian fault zone of Turkey. Ann. Tecton.6, 99–125.
Şengör, A.M.C., 1980. Türkiye'nin neotektoniğinin esasları, Türkiye Jeoloji Kurumu. Konf Ser., 40(2).
Şengör, A.M.C., Görür, N., ¸Saroğlu, F., 1985. Strike-slip faulting and related basin formation in zone of tectonic escape: Turkey as a case study. In: Biddle, K.T., Christie-Blick, N. (Eds.), Strike-Slip Deformation, Basin Deformation and Sedi-mentation. In: Spec. Publ., Soc. Econ. Paleontol. Mineral., vol.37, pp.227–264.
Sesetyan, K., Stucchi, M., V. Castelli and A.A. Gomez Capera (2023), Kahramanmaraş - Gaziantep Türkiye M7.7 Earthquake, 6 February 2023, Large historical earthquakes of the earthquake-affected region: a preliminary report, KOERI, İstanbul, Turkey.
Tan, O., Tapırdamaz, M.C., Yörük, A., 2008. The Earthquake Catalogues for Turkey. Turk. J. Earth Sci.17, 405–418.

Taymaz, T., Westaway, R., Reilinger, R. (Eds.) (2004) Active Faulting and Crustal De-formation in the Eastern Mediterranean Region. Tectonophysics 391, 1–374.

Toda, S., Stein, R. S., Özbakir, A. D., Gonzalez-Huizar, H., Sevilgen, V., Lotto, G., and Sevilgen, S., 2023, Stress change calculations provide clues to aftershocks in 2023 Türkiye earthquakes, Temblor, http://doi.org/10.32858/temblor.295

Westaway, R., Arger, J., 1996. The Gölbaşı basin, southeastern Turkey: a complex discontinuity in a major strike-slip fault zone. J. Geol. Soc.153, 729–743.

Yönlü, Ö. 2012. Doğu Anadolu Fay Zonu'nun Gölbaşı-Karataş arasındaki kesiminin Geç Kuvaterner Aktivitesi (Late Quaternary Activity of the East Anatolian Fault Zone between Gölbaşı and Karataş), Eskişehir Osmangazi Üniversitesi, Fen Bilimleri Enstitüsü.

Yönlü, Ö., Altunel, E., Karabacak, V., Akyüz, H.S., 2012. Evolution of the Gölbaşı Basin and its implications for the long term fault offset on the East Anatolian Fault Zone, Turkey, Journal of Geodynamics, 65(2013), 272-281, doi:10.1016/j.jog.2012.04.013.

Yönlü, Ö., Altunel, E. and Karabacak, V., 2017. Geological and geomorphological evidence for the southwestern extension of the East Anatolian Fault Zone, Turkey. Earth and Planetary Science Letters, 469, 1-14.

Yürür, M.T., Chorowicz, J., 1998. Recent volcanism, tectonics and plate kinematics near the junction of the African, Arabian and Anatolian plates in the Eastern Mediterranean. J. Volcanol. Geotherm. Res.85, 1–15.